J Membrane Biol (2011) 242:119–135
DOI 10.1007/s00232-011-9383-5

K^+ Channels of Squid Giant Axons Open by an Osmotic Stress in Hypertonic Solutions Containing Nonelectrolytes

Fumio Kukita

Received: 18 August 2010 / Accepted: 27 June 2011 / Published online: 21 July 2011

Abstract In hypertonic solutions made by adding nonelectrolytes, K^+ channels of squid giant axons opened at usual asymmetrical K^+ concentrations in two different time courses; an initial instantaneous activation (I_{IN}) and a sigmoidal activation typical of a delayed rectifier K^+ channel (I_D). The current–voltage relation curve for I_{IN} was fitted well with Goldman equation described with a periaxonal K^+ concentration at the membrane potential above -10 mV. Using the activation–voltage curve obtained from tail currents, K^+ channels for I_{IN} are confirmed to activate at the membrane potential that is lower by 50 mV than those for I_D. Both I_{IN} and I_D closed similarly at the holding potential below -100 mV. The logarithm of I_{IN}/I_D was linearly related with the osmolarity for various nonelectrolytes. Solute inaccessible volumes obtained from the slope increased with the nonelectrolyte size from 15 to 85 water molecules. K^+ channels representing I_D were blocked by open channel blocker tetra-butyl ammonium (TBA) more efficiently than in the absence of I_{IN}, which was explained by the mechanism that K^+ channels for I_D were first converted to those for I_{IN} by the osmotic pressure and then blocked. So K^+ channels for I_{IN} were suggested to be derived from the delayed rectifier K^+ channels. Therefore, the osmotic pressure is suggested to exert delayed-rectifier K^+ channels to open in shrinking rather hydrophilic flexible parts outside the pore than the pore itself, which is compatible with the recent structure of open K^+ channel pore.

Keywords Flexible structure · Gating · K^+ channel · Nonelectrolyte · Osmolarity · Squid giant axon · TBA

F. Kukita (✉)
Department of Cell Physiology, National Institute for Physiological Sciences, National Institutes of Natural Sciences, Nishigonaka 38, Myodaiji, Okazaki 444-8585, Japan
e-mail: kukita@nips.ac.jp

F. Kukita
Ine Marine Laboratory of National Institute for Physiological Sciences, National Institutes of Natural Sciences, Ine, Kyoto 626-0424, Japan

F. Kukita
Department of Physiological Sciences, School of Life Science, The Graduate University for Advanced Studies, Nishigonaka 38, Myodaiji, Okazaki 444-8585, Japan

Voltage-gated ionic channels are typical membrane proteins imbedded in a lipid membrane where they are controlled by the membrane potential for ions to permeate across the membrane. A recent structural analysis of voltage-gated K^+ channels (Jiang et al. 2003a, b) has suggested that the gating process does not complete only in the lipid environment (Armstrong and Hille 1998). Furthermore, voltage sensors themselves seemed to be working in hydrophilic environments because protons (Starace and Bezanilla 2004) and cations (Tombola et al. 2005, 2007; Sokolov et al. 2007) are able to permeate through the voltage sensor sheath imbedded in the membrane. However, roles of aqueous environment facing extracellular and intracellular sides of the membrane have not been analyzed extensively in the view-point that they control the gating of ionic channels because voltage sensing is generally thought to be effective in a hydrophobic lipid environment.

Concentrated nonelectrolytes first applied to a squid giant axon in order to demonstrate that the time course of ionic currents was slowed down depending on the solution microscopic viscosity (Kukita and Yamagishi 1976, 1979) and a precise mechanism for this effect was analyzed with the flexible structural model (Kukita 1997, 2000) for sodium channels, suggesting that solvent molecules near

voltage sensors should have a crucial role in the overall gating process.

Considering that the osmotic pressure shrinks some space from which solutes are segregated in cells (Van t'Hoff 1901) and macromolecules (Tanaka 1981; Rand 2004), Zimmerberg and Parsegian (1986) first demonstrated that the hypertonic solution prepared with nonelectrolyte molecules larger than the orifice of the pore decreased the open probability of ion channels (VDAC, voltage-dependent anion channel) because the pore was compressed in order to suppress their opening. Then they tried to explain the decrease of macroscopic K^+ currents of squid giant axon in hypertonic solutions by the same mechanism (Zimmerberg et al. 1990) to assess the pore interior volume. After we have known the structure of open (Doyle et al. 1998) and closed (Cuello et al. 2010) K^+ channels, it is fruitful to observe osmotic effects on neuronal voltage-gated K^+ channels carefully and analyze data with recent structural data in mind.

In this paper I report that in hypertonic solutions squid K^+ channels activated in the two different time course, i.e., the initial jump component (I_{IN}) and the delayed activating component (I_D). The component I_{IN} is attributed to open K^+ channels activated by the osmotic pressure and closed by hyperpolarization in the similar way to the component I_D. The logarithm of the ratio of these two components is proportional to the osmotic pressure and the solute inaccessible volume varied from 15 to 85 water molecules with the nonelectrolyte size. The component I_D was blocked efficiently by open channel blocker tetra-butyl-ammonium (TBA) as if in hypertonic solutions, most K^+ channels that originally showed the delayed activation kinetics in the absence of TBA were first opened by the osmotic pressure and then blocked by TBA directly without going through a delayed activation process. This osmotic effect is opposite to the osmotic suppression of channel opening (Zimmerberg et al. 1990) but is compatible to the recent 3D structure of K^+ channel pore because the osmotic pressure was supposed to rather exert on the flexible structure outside the pore than the rigid-shaped pore itself.

A preliminary report was previously published (Kukita 2001).

Materials and Methods

Axon Preparations

Squid (*Doryteuthis bleekeri, Loligo kensaki,* and *Sepioteuthis lessoniana*) were obtained at Ine, Kyoto, Japan, and kept in a circulating tank for a week before experiments. On removal from the tank, the squid were immediately killed by decapitating with fine scissors following the guidelines of animal care of National Institute for Physiological Sciences (Japan). The hindmost stellar giant axons (400–800 μm in diameter) were prepared and intracellularly perfused by a modified axoplasm squeezing method (Kukita 1997, 2000).

A periaxonal K^+ accumulation free axon (KAF axon) was obtained from a conventional intracellularly perfused axon by further perfusing externally with solutions containing additionally 0.5 to 1 M urea, which was kept constant throughout the experiment to keep an osmotic gradient (Kukita 1988).

Electrophysiology

The membrane potential was measured with a glass capillary electrode containing a floating platinum wire with asbestos-filled tip (Conti et al. 1984) and an equivalent modified tip without asbestos. Voltage clamping was performed as previously described (Kukita and Mitaku 1993). The holding potential was kept constant at −80 mV slightly below a resting membrane potential and the leakage current at this voltage was practically zero. Series of test pulses were applied from a preconditioning pulse of 0.2 to 0.8 s at −100 or −150 mV. The series resistance was made as small as possible by the proper alignment of electrodes and was carefully compensated to minimize its effects, particularly when the concentration of nonelectrolytes was increased. All membrane current data were digitized with a 12-bit A/D converter (Autonics 204C, Japan) using a sampling time of 10–40 μs after passing through a low-pass Bessel filter with a cutoff frequency from 40 to 10 KHz adjusted on the basis of the sampling theory. Data were analyzed with a microcomputer (NEC PC9801FA and PC9821V200, Japan). Most of capacitive transient was subtracted on-line using a variable transient produced in a dummy membrane circuit. Furthermore, a remaining linear capacitive response was subtracted off-line (Conti et al. 1984). After subtracting leakage with a scaling, the remaining capacitative transient and the linear leakage current were completely removed but the baseline current was the current at the preconditioning pulse (−100 or −150 mV) and current traces were shifted to adjust the zero current level at the holding potential of −80 mV (see the broken line before each trace).

The initial component of the outward current was obtained from the flat region a few hundreds μs after a transient at the instance of voltage step because this transient was contaminated with unsubtracted artifacts and gating currents.

A current measurement was performed after waiting for a longer time (15–30 min) because an exchange of viscous and hypertonic intracellular solutions takes a longer time and completed after rinsing a few times the tubing for an inlet capillary. A complete solution exchange was

monitored by the change of the capacitative transient. A continuous intracellular perfusion was checked throughout the experiments by monitoring a continuous outflow from the outlet capillary.

The temperature was maintained by circulating external solution through a heat exchange unit and all experiments were performed at approximately 10°C.

Solutions

The control external solution was TMA-ASW (TMA–artificial seawater), containing (in mM) 450 tetra-methyl-ammonium chloride (TMA-Cl), 10 KCl, 20 $CaCl_2$, 30 $MgCl_2$ and 15 Tris–HEPES (pH 8.0); 0.5 urea-TMA-ASW and 1 urea-TMA-ASW for KAF axons were TMA-ASWs containing further 0.5 and 1 M urea, respectively. A low chloride external solution 1/5 Cl–ASW was prepared by replacing TMA-Cl with TMA-Methanesulfonate. TTX (200–600 nM) was added to the external solution to remove sodium currents completely. The control internal solution was K-IS, containing (in mM) 160 KF, 40 K-phosphate, and glucose, which was used to adjust the osmolarity. Tetra-butyl-ammonium chloride (TBA) was applied to internal solutions by adding a drop of 1 M TBA solution to get a final TBA concentration.

Hypertonic solutions were prepared by adding nonelectrolytes to the external and the internal control solutions, keeping a molar concentration (M) of electrolytes equal as described in the previous paper (Kukita 1997). Various nonelectrolytes, i.e., ethylene glycol, glycerol, erythritol, glucose, sorbitol and sucrose, were used to change the osmolarity.

Hypertonic electrolyte solutions were prepared by increasing KF in the internal solution and TMA-Cl and K-Cl in the external solution in the condition that the ratio of K^+ concentration in internal and external solutions, i.e., K_O/K_I was kept constant. Isotonic solutions of a high solution resistivity were made by diluting control isotonic solutions, i.e., TMA-ASW and K-IS, with the isotonic sorbitol solution containing only pH buffer and the ratio K_O/K_I was kept constant in these solutions.

Measurement of Osmolarity

The osmolarity of solutions was measured with a freezing point osmometer (Fiske Mark 3, USA) as described in the previous paper (Kukita 1997). Osmolarities above 4000 mosmol l^{-1} were obtained by extrapolating the data as a function of the molar concentration of nonelectrolytes. The mean osmolarity of a pair of internal and external solutions was used as the solution osmolarity for the data analysis. External and internal solutions were pairs of solutions containing the same molar concentration of nonelectrolytes whose osmolarity were balanced within 5% or whose osmolarity was imbalanced to remove a periaxonal K^+ accumulation by additional urea in the external solution for KAF axons (Kukita and Yamagishi 1983; Kukita 1988). As seen in results, small urea molecules did not cause additional observable osmotic effects on K^+ channels.

Calculation for Model of TBA Blocking

A calculation of differential equations for the model described in Scheme 1 and Fig. 9C-a were performed with Mathematica 7 (Wolfram, USA). A nonlinear curve fitting was performed with FigP software (Biosoft, UK).

Results

K^+ Channels at Asymmetrical K^+ Concentrations Open Instantaneously on Depolarization More with Symmetrically Increasing Nonelectrolyte Concentrations

Typical traces of squid K^+ currents in isotonic solutions are characterized by their sigmoidal (delayed) activation on depolarization (Fig. 1A-a, B-a), which is typical of squid delayed rectifier K^+ channels (Hodgkin and Huxley 1952). As the osmolarity was increased with sorbitol, a small portion of K^+ channels was clearly activated instantaneously on depolarization (Fig. 1A-b, c, B-b, c), which was not reported by former investigators (Zimmerberg et al. 1990). Remaining K^+ channels are activated sigmoidally in a usual manner but in a slower time course with increasing the sorbitol concentration. Inward tail currents at the end of depolarization were much larger in conventional axons (Fig. 1A) than in periaxonal K^+ accumulation-free (KAF) axons (Fig. 1B) because a periaxonal K^+ accumulation was up to a few hundred millimoles in conventional axons but it was very little in KAF axons. The difference between a baseline of current trace at −100 mV prepulse and a zero current level at the holding potential of −80 mV (shown with the broken line before each current trace) was negligibly small. As listed in Table 1, the leakage current is much smaller than I_{IN} in both conventional and KAF axons and it is smaller in conventional axons than in KAF axons. After this I will designate the initial jump as I_{IN} and the delayed activating component activated with the time course designated by $t_{1/2}$ as I_D (Fig. 1D) and I_O is the sum of I_{IN} and I_D.

Looking at current–voltage relations for I_O (Fig. 1E, F), outward currents I_O decreased with sorbitol concentration without any change of the voltage dependence as reported by previous investigators (Zimmerberg et al. 1990). Current–voltage relations look roughly straight but they are composed with the activation curve of K^+ channels and the

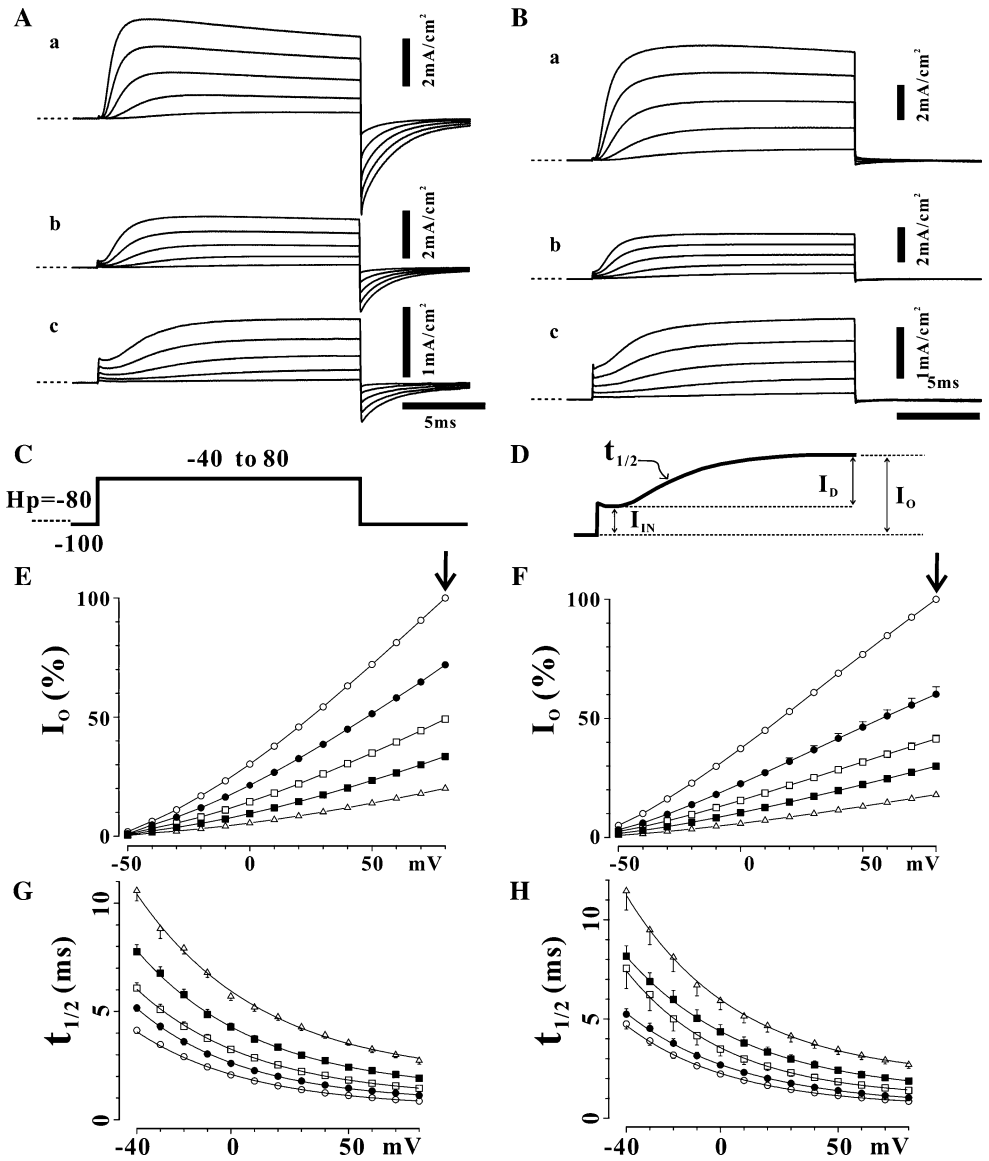

Fig. 1 Delayed activating K^+ currents in hypertonic solutions were anticipated with a stepwise activation. **A** Typical traces of K^+ currents of a conventional axon at the sorbitol concentration of (in M) 0 (*a*), 1 (*b*) and 2 (*c*), respectively. Membrane potential was changed from prepulse of −100 mV to −40 to 80 mV by 30 mV and returned to −100 mV as shown in **C**. A *broken line* before each trace was a zero current level at the holding potential of −80 mV. *Vertical bars* show 2 mA/cm^2 (*a* and *b*) and 1 mA/cm^2 (*c*). A *horizontal bar* shows 5 ms. **B** Typical traces of K^+ currents of a periaxonal K^+ accumulation free (KAF) axon (*a*–*c*). Other legends are the same as in **A**. **C** Membrane potential was changed from long prepulse of −100 mV to variable values and then returned to −100 mV, while it was usually held at −80 mV during the intermediate time. **D** Outward current (I_O) is composed of initial jump (I_{IN}) and delayed-activating component (I_D) activated with time constant of $t_{1/2}$ (half-rise time). **E** Peak K^+ currents (I_O) of a conventional axon are plotted as a function of membrane potential. Data were normalized as if I_O at 80 mV (*vertical arrow*) in control solutions was 100, and then were averaged ($n = 12$). *Error bars* are shown on one side or masked by marks. Sorbitol concentrations were (in M) 0 (*open circles*), 0.5 (*solid circles*), 1 (*open squares*), 1.5 (*solid squares*), and 2 (*open triangles*), respectively. **F** Peak K^+ currents (I_O) of KAF axons are plotted as a function of membrane potential. Averaged data ($n = 13$) with SEM are plotted in the same way as in **E**. **G**, **H** Averaged values of the activation time $t_{1/2}$ of conventional axons ($n = 12$) (**G**) and KAF axons ($n = 13$) (**H**) are plotted as a function of membrane potential with SEM. Other legends are the same as **E**

current–voltage relation of open K^+ channels and the periaxonal K^+ accumulation distorted the curve additionally in conventional axons (Fig. 1E). Even if they were obtained in KAF axons, the activation curve should be carefully obtained using the open K^+ channel current–voltage relation (Kukita 1988; Clay 1991) in place of linear current–voltage relations (Clay 2000). For these reasons, I did not perform a further analysis to obtain the activation curve but K^+ channels look to be activated above 0 mV (Fig. 1F). The activation voltage is not much different from data in a

Table 1 I_{IN} and leakage current

	Sorbitol	Sucrose	Glucose	Erythritol	Glycerol	Ethylene glycol
Conventional						
I_{IN}	3.65 ± 0.33	2.44 ± 0.46	3.61 ± 0.32	2.01 ± 0.59	3.49 ± 0.51	2.53 ± 0.52
Leak	0.09 ± 0.01	0.06 ± 0.01	0.05 ± 0.02	0.06 ± 0.01	0.02 ± 0.01	0.06 ± 0.02
	$n = 12$	$n = 7$	$n = 21$	$n = 4$	$n = 5$	$n = 4$
KAF						
I_{IN}	4.02 ± 0.41	2.25 ± 0.34	2.92 ± 0.28		3.16 ± 0.30	
Leak	0.26 ± 0.02	0.12 ± 0.01	0.03 ± 0.005		0.15 ± 0.02	
	$n = 13$	$n = 4$	$n = 6$		$n = 8$	

Slope conductances of I_{IN} after leakage subtraction and leakage currents (Leak) in mS cm^{-2} are listed at nonelectrolyte concentrations of (in M) 2, 1, 2, 2, 4 and 6 for sorbitol, sucrose, glucose, erythritol, glycerol, ethylene glycol, respectively. The slope conductance of I_{IN} was obtained between 60 and 80 mV and that for leakage currents (Leak) was obtained between −100 and −140 mV. Averaged values with SEM are listed for conventional axons and KAF axons

Table 2 Fitting parameters for Goldman equation

M	Conventional axon		KAF axon	
	K_O	Vs	K_O	Vs
0.5	12.0	−9.5	6.6	−3.9
1	14.4	8.0	9.2	2.0
1.5	13.6	17.0	17.4	−1.7
2	17.3	17.0	15.4	1.2

	M	K_O	Vs	K_O	Vs
TMA-ASW	2	18.7	16.4		
1/5 Cl^- ASW	2	19.8	8.8		

	M	K_O	Vs	K_O	Vs
I_E	2			10.2	11.5
I_{IN}	2			9.2	2.0

Top parameters obtained by fitting current–voltage relations for I_{IN} at the sorbitol concentration (in M) of 0.5, 1, 1.5 and 2 for conventional axons and KAF axons. Fitted curves are shown in Fig. 2A and B by grey lines. Averaged data ($n = 12$) of conventional axons and those ($n = 13$) of KAF axons were fitted with Goldman equation (Eq. 1). *Middle* parameters obtained by fitting current–voltage relation of I_{IN} at a sorbitol concentration of 2 M in TMA-ASW and one-fifth Cl^- ASW. Averaged data ($n = 8$) of conventional axons were fitted with Eq. 1. *Bottom* parameters obtained by fitting outward current at the end of short depolarization for 1 ms (I_E) and I_{IN} for KAF axons. Fitted curve were shown with grey lines (Fig. 2C, D). Averaged data ($n = 4$) were fitted with Eq. 1

previous report (White and Bezanilla 1985) of squid K^+ channels in which K^+ channels were reported to activate with a half activation voltage of approximately 6 mV.

Activation time constants increased with sorbitol concentrations but their voltage dependence did not change (Fig. 1G, H), which was consistent with the previous report (Zimmerberg et al. 1990).

Current–Voltage Relations of Initial Jump (I_{IN}) are Described with Goldman Equation

In an asymmetrical K^+ concentration, i.e., external K^+ concentration K_O of 10 mM and the internal K^+ concentration K_I of 200 mM, a current–voltage relation of open K^+ channel is nonlinear and was described with the Goldman equation (Kukita 1988; Clay 1991). To qualify how data are fitted with Goldman equation, I introduced an additional parameter *Vs* to the original Goldman equation. Current–voltage relations for I_{IN} were much more nonlinear than those of I_O (Fig. 2A, B) and were fitted with modified Goldman equation (Eq. 1).

$$I = Ia(V - Vs)\frac{200 - K_O\exp\left(-\frac{V}{c}\right)}{1 - \exp\left(-\frac{V-Vs}{c}\right)} \quad (1)$$

where c, K_O, and Vs are a fixed theoretical value RT/F of 24.4 mV at 10°C, an external K^+ concentration and a correction parameter, respectively.

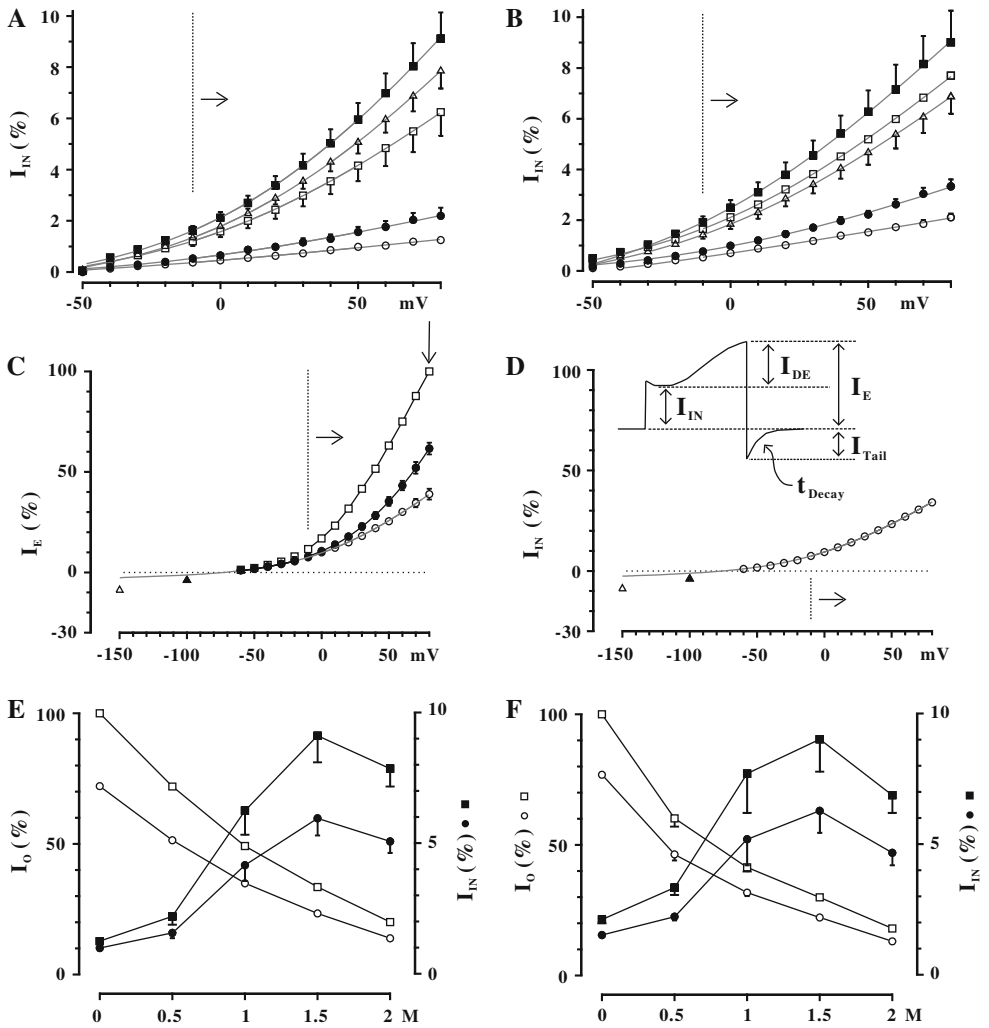

Fig. 2 The initial jump (I_{IN}) increased with sorbitol concentrations and its current–voltage relation was described with Goldman equation. **A**, **B** Averaged initial jump (I_{IN}) of conventional axons (**A**, $n = 12$) and KAF axons (**B**, $n = 13$) are plotted as a function of membrane potential with SEM, which are shown on one side or hidden by marks. Values were normalized as in Fig. 1E, F and then averaged. Data were fitted with a modified Goldman equation (Eq. 1) in a voltage range from −10 and 80 mV (shown with a *horizontal arrow* and a *vertical dotted line*) and then extrapolated. Parameters for fitting are listed in Table 2, top line. **C** Outward currents on a short depolarization for in ms 1 (*open circles*), 2 (*solid circles*), and 4 (*open squares*) are plotted as a function of membrane potential. Data were normalized to 100, at the end of 4 ms depolarization of 80 mV (*vertical arrow*) and then averaged ($n = 4$). Only I_E for 1 ms depolarization (*open circles*) were fitted with Eq. 1 in a voltage range between −10 and 80 mV (shown by the *vertical broken line* and a *horizontal arrow*) and then extrapolated. Parameters for fitting are listed in Table 2, *middle line*. Tail currents on returning to −100 mV (*solid triangles*) and −150 mV (*open triangles*) averaged at the saturating level are plotted (see Fig. 3B). **D** The initial jump (I_{IN}) is plotted as a function of membrane potential. Data are fitted with Eq. 1 and fitting parameters are listed in Table 2, *bottom line*. Other legends are the same as **C** *Inset* Definition of current components. **E**, **F** Averaged I_O (*left-hand ordinate*) and I_{IN} (*right-hand ordinate*) of conventional axons (**E**, $n = 12$) and KAF axons (**F**, $n = 13$) are plotted as a function of sorbitol concentration. Data were obtained at 80 mV (*open squares*, *open circles*) and 50 mV (*solid squares*, *solid circles*) with SEM (shown on one side or hidden by marks)

Current–voltage relations were fitted well with Eq. 1 in the voltage range between −10 to 80 mV where K^+ channels were activated fully as shown later. Because correction parameter *Vs* are close to zero, it was justified that current–voltage relations were fitted with Goldman equations (Table 1, top). K_O ranged (in mM) from 12 to 17 for conventional axons and from 7 to 17 for KAF axons (Table 1), which is slightly influenced by a different periaxonal K^+ accumulation in these preparations at the resting condition but a periaxonal K^+ accumulation is not remarkable at the start of the voltage jump comparing with those at the end of a long depolarization.

Because K_O did not change with decreasing external Cl^- to one-fifth, there was no contribution of Cl^- to I_{IN} (Table 1, middle). Replacing internal K^+ with Na^+ or TMA^+, I_{IN} decreased with I_O (data not shown).

The current–voltage relation for I_E at 1 ms was quite different from those at 2 and 4 ms and could be fitted with

Goldman equation (Fig. 2C) as that of I_{IN} (Fig. 2D) because a delayed activating component was not yet activated (Table 1, bottom). Obtained K_O was roughly equal to the K^+ concentration in the external solution (i.e., 10 mM) which means that the reversal potential is approximately −73 mV. Although tail currents at the saturated level was slightly below the extrapolated curve for I_E (1 ms) and I_{IN}, the current–voltage relation for I_{IN} are remarkably nonlinear and the current is really reversed at the membrane potential near E_K.

I_O and I_{IN} changed with sorbitol concentrations in a reverse fashion (Fig. 2E, F); I_O decreased but I_{IN} increased with sorbitol concentrations. Because I_{IN} has a peak around 1.5 M, the number of K^+ channels activated is suggested to increase osmolarity-dependently while single K^+ channel conductance decreased in the same manner as in I_O with sorbitol concentration.

K^+ Channels Contributing I_{IN} are Activated at the Membrane Potential Lower by 50 mV than Those Contributing I_D

Comparing with tail currents on returning the membrane potential to −100 mV (Fig. 1B-a–c), tail currents on returning to −150 mV were large enough for a further analysis (Fig. 3A). To clarify the characteristics of I_{IN} separately with those of I_D, the tail current after the short depolarization was recorded with increasing the population of I_D. Because a short depolarization from −150 mV for 1 ms did not activate I_D, tail currents observed were mainly attributed to I_{IN} (Fig. 3A-a).

An activation curve could be estimated from tail current records, even if the current–voltage relation was nonlinear. The amplitude of tail current before the delayed activating component appeared could be fitted with Eq. 2 (Fig. 3B) with fitting parameters (Table 3).

$$I = \frac{I_{Max}}{1 + \exp\left(-K\left(V - V_{1/2}\right)\right)} \quad (2)$$

where I_{Max}, K, and $V_{1/2}$ are a maximum current, a parameter for steepness, and a half-activation voltage, respectively.

I_{IN} was activated with the half-activation voltage of approximately −50 mV and the delayed activating component was activated at much higher membrane potential.

The time constants (t_{Decay}) of the closing process of I_{IN} increased slightly with a depolarizing voltage (Fig. 3C, 1 ms) in the range where only I_{IN} is observed but markedly increased (Fig. 3C, 2 and 4 ms) as the population of I_D increased.

The population of I_D at the end of a short depolarization was redefined as I_{DE}/I_{IN} using I_{DE} (Eq. 3) in place of I_D.

$$I_{DE} = I_E - I_{IN} \quad (3)$$

where I_{DE} and I_E are the delayed-activating component and the K^+ current at the end of a short depolarization, respectively.

The decay time constants (t_{Decay}) were plotted against I_{DE}/I_{IN}, which increased with the duration and the magnitude of depolarization (Fig. 3D). Considering that the decay time constant was a kind of a weighted average of time constants of I_{IN} and I_{DE}, the decay time constant should depend on I_{DE}/I_{IN}. When I_{DE}/I_{IN} is less than 0.5, decay time constants are mainly attributable to those of I_{IN} and they increased in proportion to I_{DE}/I_{IN}. Although the dependence on I_{DE}/I_{IN} seemed to be slightly weaker for a longer depolarization (Fig. 3D-b, 4 ms), the decay time constants of the initial jump component I_{IN} also increased with time as explained by the activation process Scheme 1. The delayed rectifier K^+ channels are thought to be activated by depolarization through many successive closing states in Scheme 1 (Gilly and Armstrong 1982; Hille 2001) and the kinetics of closing processes is also affected where K^+ channels occupy in intermediate closing states.

$$C_0 \rightleftarrows C_1 \rightleftarrows C_2 \quad \rightleftarrows \quad \rightleftarrows \quad C_n \rightleftarrows O$$

Scheme 1

where C_k's and O are successive closed states and a final open state.

Therefore, I_{IN} could close through the similar closing pathway controlled by the voltage sensor.

I_{IN} for Various Nonelectrolytes Decreased with Decreasing Osmolarity

On reducing a sorbitol concentration from 2 to 0 M in the same axon as in Fig. 1B, the current amplitude increased and their time course became faster (Fig. 4A). Values of I_{IN} were roughly doubled but they were much smaller than those at sorbitol concentration of 2 M. Decreasing nonelectrolyte concentrations was much more difficult because it took a longer time than increasing nonelectrolyte concentration and must be carefully performed not to damage axons. For these reasons, the magnitude of I_O was restored to only 65% of that in control solutions at the beginning of each experiment. However, it is difficult to say that lost K^+ channels may contribute to the increase of I_{IN}.

Average values of I_{IN} at the start and at the end of experiments with the maximum values of I_{IN}, which were observed at the second maximum concentration but not the maximum concentration (Fig. 4B). I_{IN} recovered almost to the initial level in conventional axons (Fig. 4B-a) but it recovered poorly in KAF axons (Fig. 4B-b). However, it was clear that I_{IN} decreased with decreasing osmolarity

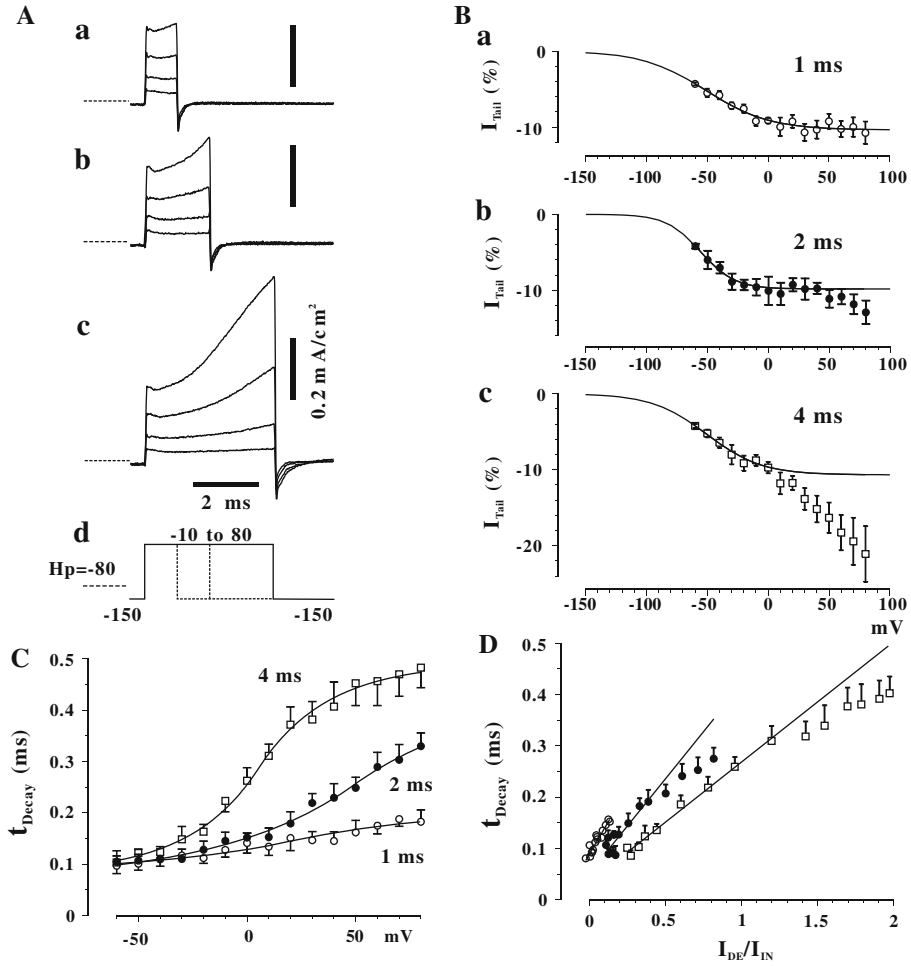

Fig. 3 Initial jumps were activated voltage dependently. **A** K^+ currents activated with a short depolarization of (in ms) 1 (*a*), 2 (*b*), and 4 (*c*) in 2 M sorbitol solutions were accompanied with inward tail currents at the end of depolarization. A membrane potential was depolarized from (in mV) −150 to −40, −10, 20, and 50 and returned to −150 mV as shown in (*d*). A zero current level at the holding potential of −80 mV is indicated by a *horizontal broken line* before each family of traces. *Vertical and horizontal bars* show 0.2 mA/cm^2 and 2 ms, respectively. **B** Amplitudes of tail current (I_{Tail}) at the end of a short depolarization for (in ms) 1 (*a*), 2 (*b*), and 4 (*c*) are plotted as a function of amplitude of the short depolarization. Tail currents were obtained as if I_E at the end of 4 ms depolarization of 80 mV was normalized to 100 (shown by a *vertical arrow* in Fig. 2C) and then averaged ($n = 4$). Averaged data with SEM were fitted with Eq. 2 with parameters listed in Table 3. Tail currents saturated at around −10, before the delayed activating component was remarkable. **C** Decay time constants of inward tail currents (t_{Decay}) are plotted as a function of the amplitude of short depolarization. t_{Decay}s were obtained by fitting tail current traces with a single exponential function (see inset of Fig. 2D). Averaged data ($n = 4$) with SEM (shown on one side) are plotted. The duration of depolarization was (in ms) 1 (*open circles*), 2 (*solid circles*), and 4 (*open squares*). **D** t_{Decay}s are plotted as a function of I_{DE}/I_{IN}. I_{DE} was the delayed-activating component partially activated at the end of a short depolarization (as shown in the inset of Fig. 2D), which was much smaller than a fully activated level I_D shown in Fig. 1D. Values of I_{DE}/I_{IN} were close to zero during a short and small depolarization and progressively increased as a delayed-activating component became remarkable. Other legends are the same as in **C**

Table 3 Parameters of activation curve for I_{IN}

ms	$V_{1/2}$	I_{Max}	K
1	−51.0	−10.3	0.038
2	−55.9	−9.8	0.072
4	−50.4	−10.7	0.044

Parameters obtained by fitting activation–voltage curves (Fig. 3C-a, b, c) with Eq. 2. I_{Max}, K and $V_{1/2}$ are a maximum current, a parameter for steepness and a half-activation voltage, respectively

even if the osmotic pressure was increased with any nonelectrolytes.

Ratio of I_{IN} to I_O Does not Depend on the Membrane Potential

Because the single channel conductance of K^+ channel was reported to decrease by a unilateral application of hypertonic solution from the inside of K^+ channels (Starkus et al.

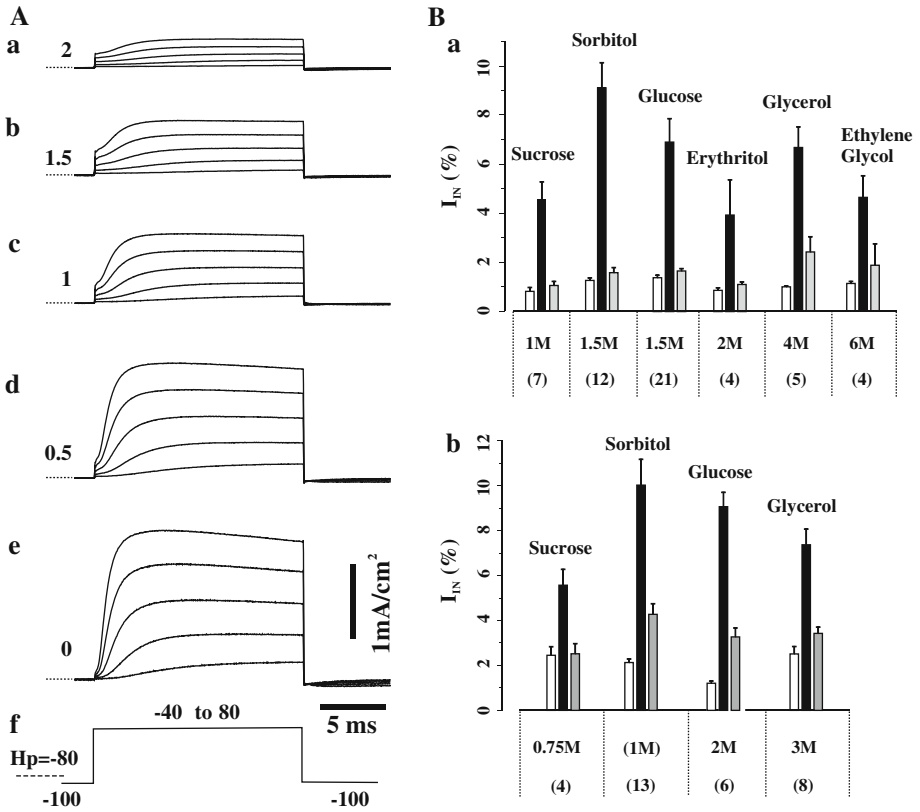

Fig. 4 Effects of hypertonic solutions were reversible. **A** K^+ currents decreased on reducing sorbitol concentration from 2 to 0 M. I_{IN} decreased markedly while I_O increased with accelerating the activation time course. Sorbitol concentrations were (in M) 2, (*a*), 1.5 (*b*), 1 (*c*), 0.5 (*d*), and 0 (*e*) (*left*). A *broken line* before each family of traces is a zero current level at the holding potential of −80 mV. *Vertical and horizontal bars* show 1 mA/cm^2 and 5 ms. Traces from the same axon as in Fig. 1B were shown. **B** I_{IN}s for various nonelectrolytes were recovered when hypertonic solutions were restored to isotonic solutions. Three bars with SEM for each nonelectrolyte show the control (*left, white bar*), the maximum value (*middle, black bar*), and the recovered value (*right, gray bar*). Nonelectrolytes are indicated above bars with their concentration in M at which I_{IN} has a maximum value below bars. When the maximum value was during the returning course to 0 M, it was parenthesized. The number of experiments is shown in parenthesis. Data of conventional axons (*a*) and KAF axons (*b*) are shown

1995; Shimizu and Oiki 2004), it could be supposed that the single channel conductance decreases by the nonelectrolyte application from both sides. Furthermore, the entrance of the open pore of K^+ channel (Cuello et al. 2010) looks wide enough for nonelectrolytes to enter into it to decrease the single channel conductance. Assuming that species of K^+ channels and then their single channel properties were the same in K^+ channels for I_{IN} and I_D, the ratio of I_{IN} to I_O was interpreted to be the ratio of K^+ channels contributing to I_{IN} in total K^+ channels. Plotting this ratio as a function of membrane potential (Fig. 5A, C), it is concluded that this ratio increased with a sorbitol concentration but not dependent on membrane potential suggesting the previous assumption was correct.

In place of I_{IN}/I_O, the ratio of I_{IN} to I_D (I_{IN}/I_D) is plotted as a function of membrane potential (Fig. 5B, D). Values of I_{IN}/I_D are slightly voltage dependent but are strongly dependent on sorbitol concentration. Data obtained from conventional axons and KAF axons are quite similar, even though leakage currents of these axons were different.

Considering normal transition states of K^+ channels are successive closing states coupling with voltage-sensors, a transition to produce I_{IN} should occur in the early stages. K^+ channels in the state C_k are equilibrated with those in the state $C_k(\Pi)$ with the equilibrium constant K_{EQ} as Eq. 5.

$$C_k \rightleftarrows C_k(\Pi) \tag{4}$$

$$K_{EQ} = \frac{I_{IN}}{I_D} \tag{5}$$

where k is the number of intermediate state in Scheme 1.

Because K^+ channels in any intermediate states were affected by the osmotic pressure, the sum of K^+ channels opened by the osmotic pressure can be considered to be equal to the initial value K_{EQ} at time of 0 because C_k varies time dependently with the sum of all states to be equal to unity in Scheme 1.

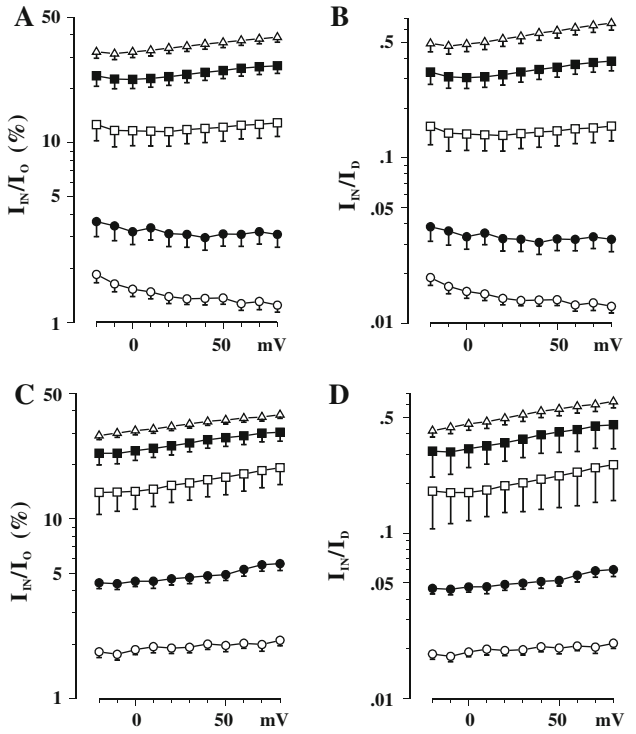

Fig. 5 I_{IN}/I_O and I_{IN}/I_D are independent of membrane potential. **A, B** I_{IN}/I_O and I_{IN}/I_D on a logarithmic scale are plotted as a function of membrane potential. Sorbitol concentrations were (in M) 0 (*open circles*), 0.5 (*solid circles*), 1 (*open squares*), 1.5 (*solid squares*), and 2 (*open triangle*). Data of conventional axons (**A**, **B**) ($n = 12$) and those of KAF axons (**C**, **D**) ($n = 13$) are plotted with SEM, which was shown on one side

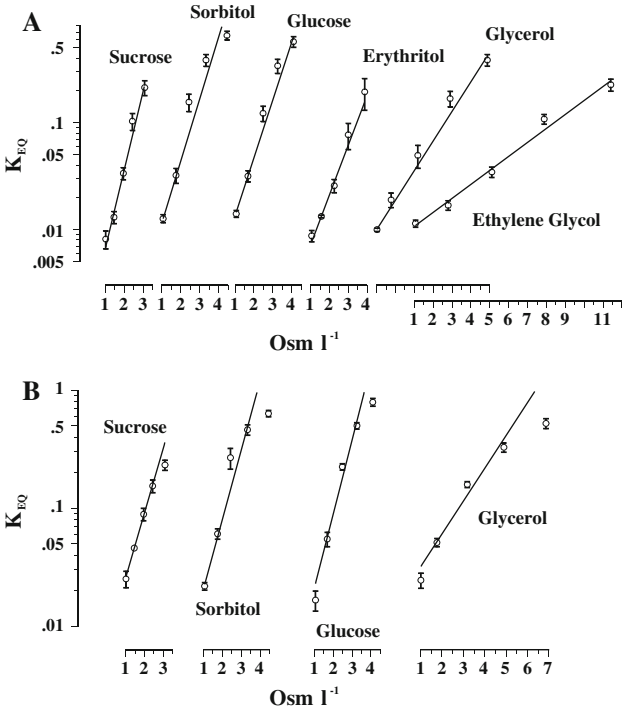

Fig. 6 Logarithmic values of K_{EQ} are linearly related with osmolarity. **A** K_{EQ}s on a logarithmic scale are plotted as a function of osmolarity. Data for each nonelectrolyte are shifted horizontally with the abscissa for clarity. K_{EQ}s at 80 mV on a logarithmic scale are plotted as a function of osmolarity (osmol l^{-1}) with SEM, which are shown in one direction or hidden by marks. Data of conventional axons were fitted with Eq. 6. Nonelectrolyte species are shown near the data. **B** Data of KAF axons are plotted as a function of osmolarity, which was the osmolarity of solutions without urea (the same osmolarity as in **A**) in place of a measured osmolarity of solutions containing urea

Equilibrium Constant K_{EQ} is Dependent on Solution Osmolarity

The equilibrium constant K_{EQ} for a different size of nonelectrolytes was plotted on the logarithm scale as a function of osmolarity and could be fitted with Eq. 6 (Fig. 6).

$$K_{EQ} = K_C \cdot \exp(\beta \cdot \Delta\Pi) \tag{6}$$

where K_C, β and $\Delta\Pi$ are an equilibrium constant in control solutions, a slope of data on the logarithmic plot and a difference in osmolarity of hypertonic solutions from that of control solutions, Π–Π_0 in osmol/l, respectively.

The equilibrium constant (K_{EQ}) is described generally as in Eq. (7).

$$K_{EQ} = \exp\left(\frac{\Delta G}{RT}\right) \tag{7}$$

$$\Delta G = V_{INA} \cdot \Delta\Pi \tag{8}$$

where ΔG, $\Delta\Pi$, and V_{INA} are a free energy difference, Π–Π_0 in N m^{-2} and a solute accessible volume in m^3, respectively, and R and T are the gas constant and the absolute temperature. The equilibrium constants K_{EQ} obtained from KAF axons were quantitatively similar to those from conventional axons (Fig. 6B).

Solute Inaccessible Spaces are Distributed Outside the Pore

As shown in Eqs. 6 and 7, the slope β is the solute inaccessible volume in l/mol and dividing β by Avogadro's number N_a, the solute inaccessible volume (in $Å^3$) for one K^+ channel was obtained.

The number of water molecules per one K^+ channel was obtained as expressed with Eq. 9.

$$N_W = \frac{V_{INA}}{V_W} \tag{9}$$

where V_w is the volume of one water molecule.

Because the solute inaccessible volume V_{INA} and the number of water N_W were obtained at a variable membrane potential and did not depend significantly on membrane potentials, they were averaged between 0 and 80 mV for various nonelectrolytes are plotted as a

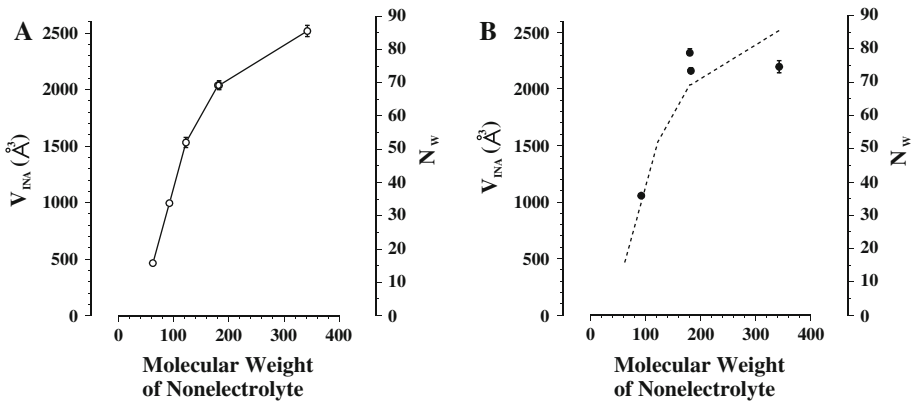

Fig. 7 A solute inaccessible volume V_{INA} increased with the molecular weight of nonelectrolytes. **A** V_{INA}s of conventional axons are plotted as a function of molecular weight of nonelectrolytes. Values at variable voltages are averaged between 0 and 80 mV for each nonelectrolyte. The *left-hand ordinate* shows V_{INA} in Å^3 and the *right-hand ordinate* shows the number of water molecules that can occupy this volume. Data of glucose and sorbitol are overlapped. **B** V_{INA}s of KAF axons are plotted as a function of molecular weight of nonelectrolytes. A *dotted line* shows the data of **A**

function of nonelectrolyte molecular weight (Fig. 7). Similar values of V_{INA} was obtained when data were plotted as a function of osmolarity of the corresponding control solutions ignoring the contribution of urea because urea was as small as ethylene glycol to cause the osmotic effects.

The number of water molecules varies from 13 to 85 depending on the molecular size and there was not a cutoff in its size. Variable solute inaccessible spaces might be distributed in parts outside the pore.

I_{IN} was not Observed in Both Hypertonic Electrolyte Solutions and Isotonic Solutions with a Lower Electrolyte Concentration

Nonelectrolytes in hypertonic solutions inevitably increase the solution resistivity even if electrolyte molar concentrations were equal throughout experiments. I performed two experiments to check the effect of the solution resistivity; experiments in hypertonic electrolyte solutions (Fig. 8A–C) and those in isotonic solutions whose electrolyte were replaced partly with sorbitol in order to increase the solution resistivity (Fig. 8D–F).

Increasing the osmolarity with keeping the ratio of K^+ concentrations in external and internal solutions (K_O/K_I) equal, K^+ currents increased (Fig. 8A-b) without observable I_{IN} (Fig. 8B). A remarkable I_{IN} was observed at K_I of 1 M but the ratio of I_{IN} to I_O was as small as could be explained by the osmotic effect of small molecules comparing with data for ethylene glycol (Fig. 7A). Time constants increased in hypertonic electrolyte solutions (Fig. 8C) by about twofold as described by previous investigators (Wagoner and Oxford 1987), but was smaller than in hypertonic nonelectrolyte solutions (Fig. 1E, F).

When electrolytes were replaced with nonelectrolytes keeping both the solution osmolarity and the ratio of K^+ concentrations (K_O/K_I) constant, the solution resistivity increased up to eightfold, which was more than that of hypertonic solutions containing nonelectrolytes in which the solution resistivity increased at most by 3.5-fold. In these isotonic solutions, K^+ currents decreased with decreasing K_I (Fig. 8D-a–c) but the current trace showed typical characteristics of a delayed-activating kinetics without initial jumps. In solutions whose solution resistivity was increased by about eightfold (Fig. 8B-c), I_{IN} was not observable (Fig. 8E). Therefore, it is concluded that osmotic effects of nonelectrolytes are not affected by an inevitable increase of the solution resistivity.

TBA Blocks I_D in Hypertonic Solutions in Fast Blocking Process Rather than in Normal Slow Process

If K^+ channels for I_{IN} and I_D are derived from different species of K^+ channels, they are blocked by open channel blockers independently of each other, changes in population by the application of K^+ channel blocker TBA (tetrabutyl ammonium) means that K^+ channels can be converted to each other and then it is concluded that K^+ channels for I_{IN} and I_D are derived from the same molecular species.

TBA is well-known open K^+ channels blocker with the typical blocking kinetics (Fig. 9C-a) (French and Shoukimas 1981; Hille 2001; Li and Aldrich 2004; Yahannan et al. 2007), which was confirmed for K^+ channels in isotonic solutions (blue traces in Fig. 9A). Typical characteristics are that K^+ currents in the presence of TBA (blue traces in Fig. 9A) overlap with those in the absence of TBA (black traces in Fig. 9A) in the rising phase and are

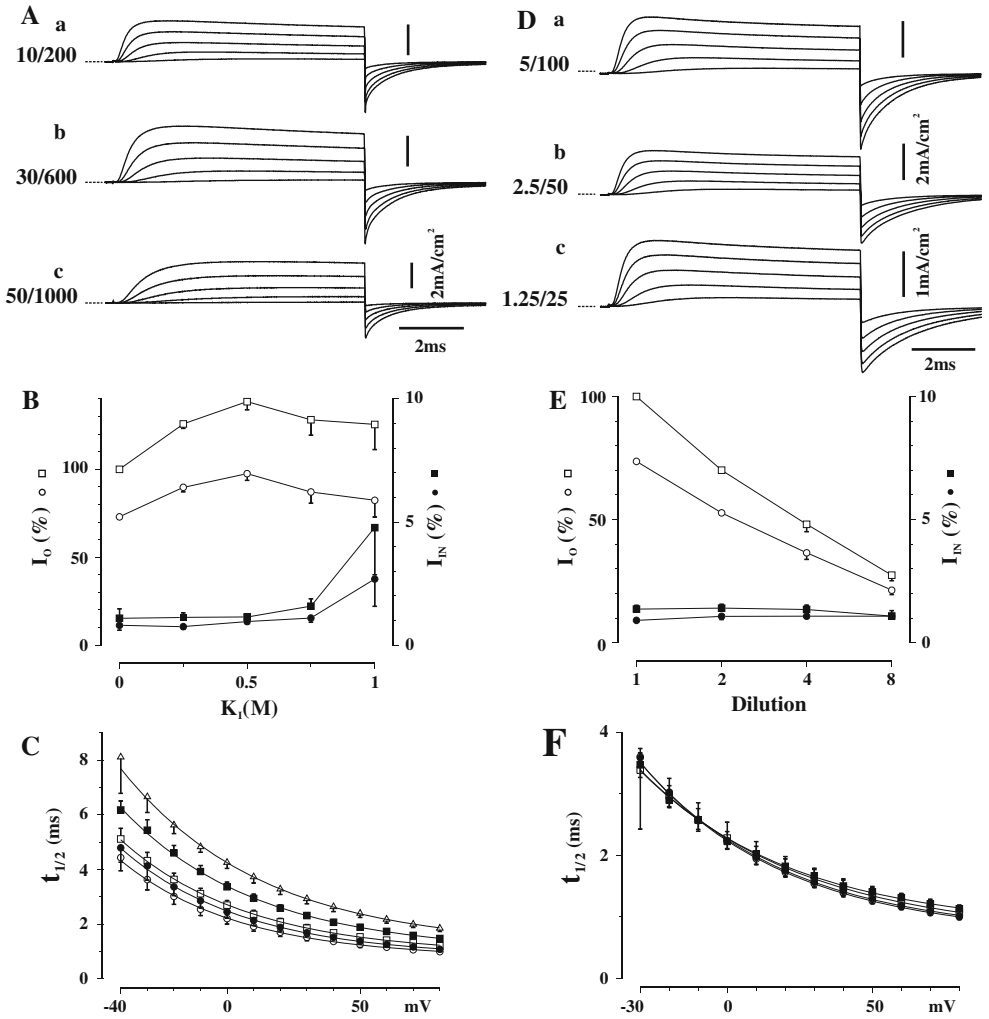

Fig. 8 I_{IN} was not observed in hypertonic solutions with increased electrolytes and in isotonic solutions with decreased electrolytes. **A** K^+ currents of the conventional axon in hypertonic solutions containing concentrated electrolytes have not remarkable I_{IN}s (*b* and *c*). Electrolytes were increased with ratios of internal and external K^+ concentrations equal. K_O/K_I were (in mM) 10/200 (*a*), 30/600 (*b*), and 50/1000 (*c*). A membrane potential was depolarized from a prepulse of −100 mV to (in mV) −40, −10, 20, 50, and 80. *Vertical and horizontal thick bars* on the right side show 2 mA/cm^2 and 2 ms. **B** I_O and I_{IN} are plotted as a function of K_I. I_O at 80 mV (*open squares*) and 50 mV (*open circles*) are shown on the *left-hand ordinate* and I_{IN} at 80 mV (*solid squares*) and 50 mV (*solid circles*) are shown on the *right-hand ordinate*. Data with SEM (shown on one side or masked by marks) are plotted ($n = 5$). **C** Activation time constants ($t_{1/2}$) are plotted as a function of membrane potential. K_O/K_I are (in mM) 10/200 (*open circles*), 20/400 (*solid circles*), 30/600 (*open squares*), 40/800 (*solid squares*), and 50/1000 (*open triangles*). Data with SEM (shown on one side or masked by marks) are plotted ($n = 5$). **D** K^+ currents of the conventional axon in isotonic solutions had not I_{IN}s (*a*, *b*, and *c*), while K^+ current decreased with decreasing K^+ concentration. Electrolytes in TMA-ASW and K-IS were diluted with isotonic sorbitol solutions containing only pH buffers. At the same time, the solution resistivity increased. Ratios K_O/K_I were kept equal and were (in mM) 5/100 (*a*), 2.5/50 (*b*), and 1.25/25 (*c*). A membrane potential was depolarized from a prepulse of −100 mV to (in mV) −40, −10, 20, 50, and 80. *Vertical thick bars* on the right hand are (in mA/cm^2) 2 (*a* and *b*) and 1 (*c*), and a *horizontal thick bar* shows 2 ms. **E** I_O and I_{IN} are plotted as a function of a degree of dilution. I_O at 80 mV (*open squares*) and 50 mV (*open circles*) are shown on the *left-hand ordinate* and I_{IN} at 80 mV (*solid squares*) and 50 mV (*solid circles*) are shown on the *right-hand ordinate*. Data with SEM (shown on one side or masked by marks) are plotted ($n = 4$). **F** Activation time constants ($t_{1/2}$) are plotted as a function of membrane potential. Ratios (K_O/K_I) are (in mM) 10/200 (*open circles*), 5/100 (*solid circles*), 2.5/50 (*open squares*), and 1.25/25 (*solid squares*). Data were not significantly different and then overlapped. Data with SEM (shown on one side or masked by marks) are plotted ($n = 4$)

explained by the blocking mechanism that K^+ channels were activated normally and then blocked after they opened (French and Shoukimas 1981; Hille 2001) (Fig. 9C-a). The model calculation shows the same blocking profile (Fig. 9B).

Comparable traces for I_D in hypertonic solutions were easily observed after current traces were shifted upward (red traces in Fig. 9E) but they increased much slowly because K^+ channels were already blocked before they were fully activated (Fig. 9C-b fast). A population of K^+

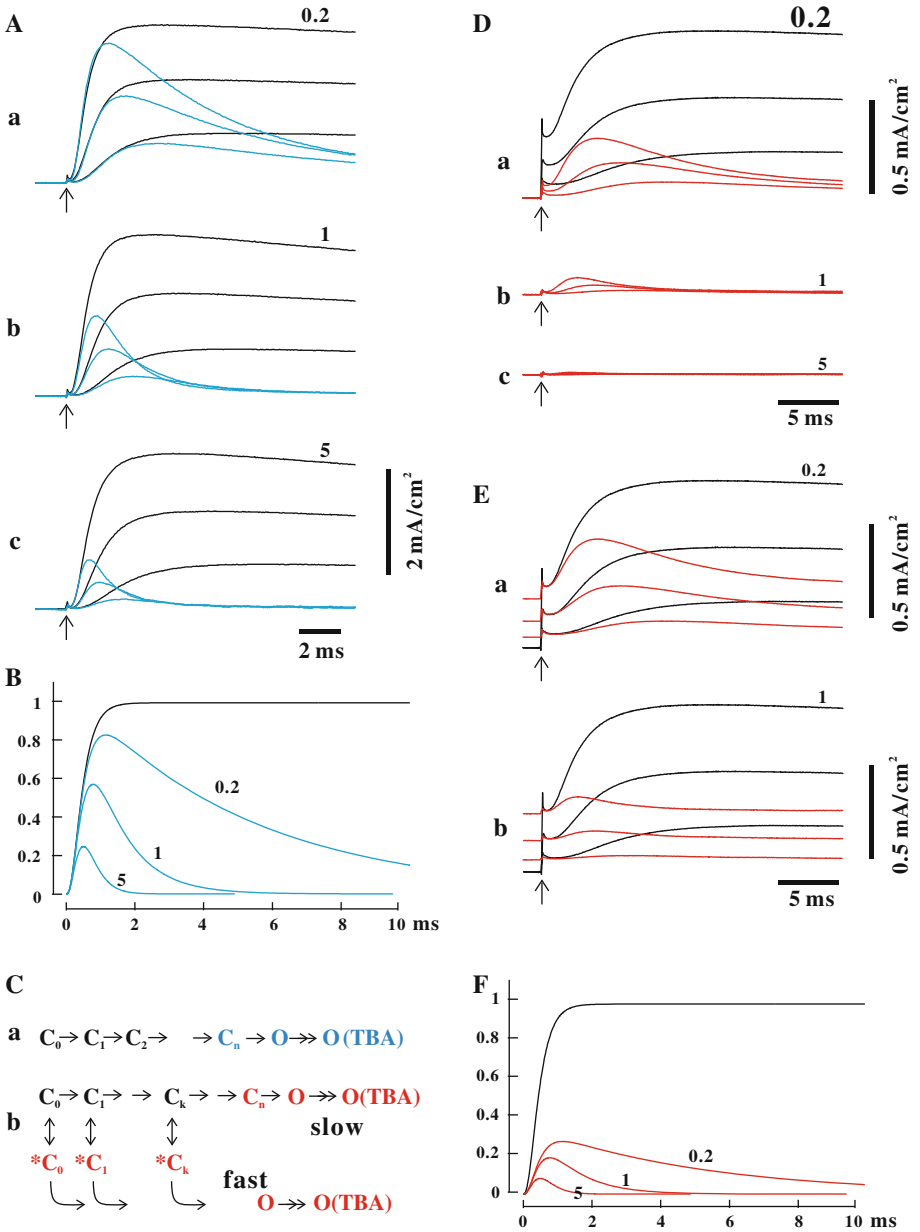

Fig. 9 Open K^+ channel blocker TBA suppressed both I_{IN} and I_D but in a different way. **A** K^+ currents of conventional axon in the presence of TBA (tetra-butyl ammonium) in the internal solution (*blue traces*) are shown comparing with control K^+ currents in the absence of TBA (*black traces*) on the same horizontal and vertical scales. A membrane potential was changed from −100 mV to 0, 40, and 80 mV at the instance shown with an *upper arrow*. *Black* and *blue traces* are depicted on the same *horizontal and vertical scales* and the baseline of *blue and black traces* are the same for each TBA concentration. *Vertical and horizontal bars* on the right hand show 2 mA/cm^2 and 2 ms, respectively. Numbers above each trace show TBA concentration in mM. **B** Current traces (*blue traces*) calculated according to the model (**C**-*a* and **C**-*b* slow) in which K^+ channels were blocked by TBA after they opened along the delayed activating pathway. Blocking rates were increased in proportional to TBA concentration. The *black trace* is that in the absence of TBA. **C** The scheme that TBA blocks K^+ channels in isotonic solutions (*a*) and in hypertonic solutions (*b*). $*C_k$s are equal to $C_k(\Pi)$s in Eq. 4. **D** K^+ currents in hypertonic solutions containing 2 M sorbitol were suppressed by TBA (*red traces*). Current traces in the absence of TBA (*black traces*) were shown on the same scale (*a*). As TBA concentration increased (in mM) to 0.2 (*a*), 1 (*b*), and 5 (*c*), currents decreased concentration dependently. *Vertical and horizontal bars* on the right hand of traces show 0.5 mA/cm^2 and 5 ms, respectively. **E** Current traces in the presence of TBA (*red traces* in **B**) were represented by shifting upward for a rising phase of I_D to be matched to traces in the absence of TBA (*black traces*) at the start of depolarization (*upper arrow*). Horizontal red traces before the voltage change show the corresponding baseline shift. Current traces (*red traces*) in the presence of 0.2 (*a*) and 1 mM TBA (*b*) were presented on the same vertical and horizontal scales. Other legends are the same as in **A**. **F** Current traces calculated in which K^+ channels were blocked by TBA both in slow and fast blocking pathways (**C**-*b*). These were obtained with reducing the initial value to one-third of that in **B**. The *black trace* is that in the absence of TBA

channels blocked in a usual slow blocking time course (Fig. 9C-b slow) decreased with TBA concentration as shown in Fig. 9F.

I_{IN} in hypertonic solutions was remarkably blocked by TBA as shown in the baseline shift (Fig. 9C) because K^+ channels were open even at this early stage (Fig. 9C-b).

TBA Suppressed K^+ Currents More Effectively in Hypertonic Solutions

I_D was blocked by TBA in the isotonic solutions and in hypertonic solutions independently of the membrane potential (Fig. 10A) because TBA blocked K^+ channels at the end of the activation time course. Initial jump (I_{IN}) were blocked more effectively than I_O because K^+ channels for I_{IN} were opened steadily above 0 mV (Fig. 10B).

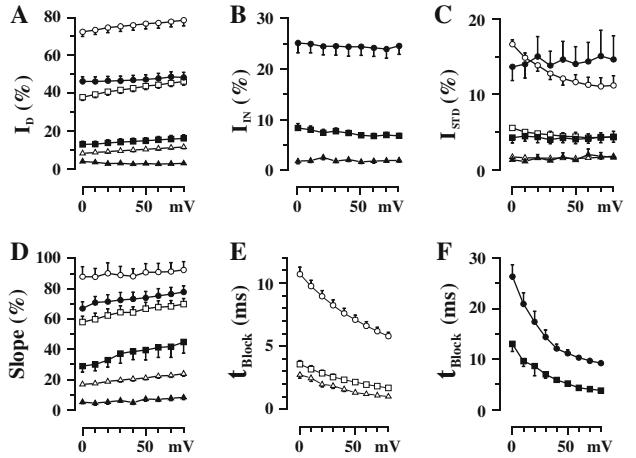

Fig. 10 TBA blocks K^+ components independently of membrane potential. **A** Percentage changes of I_D with the application of TBA in the isotonic solutions (*open marks*) and in hypertonic solutions containing 2 M sorbitol (*solid marks*) are plotted. Values of I_D in the absence of TBA are normalized to 100 in isotonic and hypertonic solutions at each membrane potential (not shown). TBA concentrations are (in mM) 0.2 (*circles*), 1 (*squares*), and 5 (*triangles*). Data in isotonic solutions ($n = 6$) and those in hypertonic solutions ($n = 8$) are plotted with the SEM. **B** Percentage change of I_{IN} in hypertonic solutions are shown at the TBA concentration of (in mM) 0.2 (*solid circles*), 1 (*solid squares*) and 5 (*solid triangles*). Values of I_{IN} in the absence of TBA are normalized to 100, at each membrane potential (not shown). **C** Percentage changes of steady currents (I_{STD}) are plotted as a function of membrane potential. *Open marks* show steady currents in isotonic solutions, and *solid marks* show those in hypertonic solutions. TBA concentrations are (in mM) 0.2 (*circles*), 1 (*squares*), and 5 (*triangles*). Steady currents in the absence of TBA are normalized to 100, at each membrane potential (not shown). **D** The maximum slope in the rising phase of K^+ current trace is plotted as a function of the membrane potential. The slope of K^+ current in the absence of TBA is normalized to 100, at each membrane potential. **E**, **F** TBA blocking time constants (t_{Block}) are plotted with SEM as a function of membrane potential in isotonic solutions (*open marks,* **E**) and in hypertonic solutions (*solid marks,* **F**). They were obtained from a current decay after the peak in the presence of TBA. TBA concentrations are (in mM) 0.2 (*circles*), 1 (*squares*), and 5 (*triangles*)

The blocking of the total K^+ current (I_O) by TBA at the end of the long depolarization for up to 64 ms (I_{STD}) was almost equal in both isotonic and hypertonic solutions (Fig. 10C) at higher TBA concentration and the affinity of TBA does not look different in isotonic and hypertonic solutions. The maximum slope during activation decreased much more markedly in hypertonic solutions than in isotonic solutions (Fig. 10D).

The blocking time constants t_{Block}s decreased with membrane potential because the activation time constant increased with membrane potential, while the blocking rate increased with TBA concentration (Fig. 10E, F). The blocking time constants were larger in hypertonic solutions by three times (Fig. 10F) than those in isotonic solutions (Fig. 10E) because the activation is slower in hypertonic solutions.

I_{IN} was blocked by TBA less than I_{STD} but it was blocked to the same extent as TBA concentration increased (Fig. 11A). On the other hand, I_D was blocked more efficiently in hypertonic solutions than those in isotonic solutions (Fig. 11B) and the difference of I_D and the maximum slope of the activation were enlarged (Fig. 11C) with TBA concentration. Because t_{Block}s are correlated with $t_{1/2}$s at variable TBA concentration (Fig. 11D), the initial value of I_D is estimated by extrapolating the blocking curve to time zero. This initial value in hypertonic solutions was approximately 25% of that in isotonic solutions (Fig. 11E) at TBA concentration of 1 mM corresponding that 75% of I_D was converted to I_{IN} to be blocked. At TBA concentration of 5 mM, I_D was 3% (Fig. 11B) and almost K^+ channels were supposed to be blocked in the fast pathway (the broken line in Fig. 11F).

Discussion

K^+ currents in concentrated nonelectrolyte solutions are characterized with their initial stepwise activation I_{IN} preceding a usual sigmoidal activation I_D at usual asymmetrical K^+ concentrations. This was explained that squid delayed rectifier K^+ channels, which usually activate on depolarization in a sigmoidal and delayed activation kinetics in the isotonic solutions are partly opened by the osmotic pressure. These K^+ channels close at the membrane potential below the resting membrane potential and activate at the membrane potential by 50 mV lower than the usual activation voltage of the squid delayed rectifier K^+ channels. Closing time constants for I_{IN} obtained by tail currents vary with the amplitude and the duration of the preceding depolarization in the similar way to those of I_D.

Using TBA blocking kinetics typical of open channel blockers (French and Shoukimas 1981; Hille 2001; Li and Aldrich 2004), the population of K^+ channels contributing

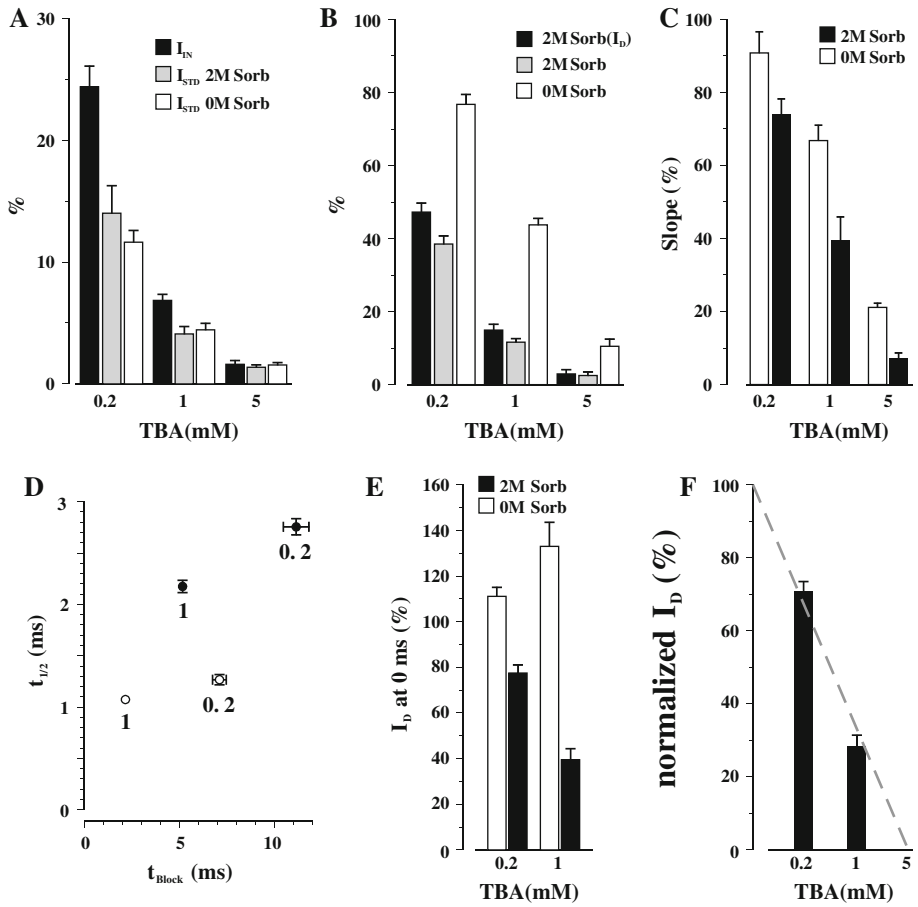

Fig. 11 TBA blocks I_D efficiently in hypertonic solutions. **A** Percentage changes of I_{IN} in hypertonic solutions containing 2 M sorbitol (*black bars*) with those of steady currents (I_{STD}) in hypertonic solutions (*gray bars*) and in isotonic solutions (*white bars*) are plotted as a function of TBA concentration. Averaged values at 50 mV in hypertonic solutions ($n = 8$) and those in isotonic solutions ($n = 6$) are shown with SEM. **B** Percentage changes of (I_D) in hypertonic solutions (*black bars*) and those of peak K^+ currents (I_O) in isotonic solutions (*white bars*) and in hypertonic solutions (*gray bars*) are plotted as a function of TBA concentration. In isotonic solutions, I_D was equivalent to I_O because I_{IN} was zero. **C** Percentage changes in the maximum slope of rising phase in isotonic and hypertonic solutions in the present of TBA. **D** Activation time constants of I_D ($t_{1/2}$) are plotted as a function of blocking time constants (t_{Block}). An activation time constant $t_{1/2}$ was defined by a half-rise time of I_D. *Open circles* show data in isotonic solutions with SEM and *solid circles* show those in hypertonic solutions. Figures along data show TBA concentration in mM. **E** I_Ds at the start (0 ms) in isotonic solutions (*open bars*) and in hypertonic solutions (*solid bars*) are plotted as a function of TBA concentration. I_D at the time of 0 ms was estimated as $I_D \cdot \exp(2t_{1/2}/t_{Block})$. **F** The percentage of K^+ channels that were blocked in the slow pathway (Fig. 9C-a) was estimated by dividing values in hypertonic solutions by the corresponding value in isotonic solutions at the same TBA concentration. A *gray dotted line* is drawn assuming that 100% of I_D is blocked by TBA at 0.04 mM and 0, at 5 mM

I_D in hypertonic solutions was estimated. If K^+ channels contributing to I_{IN} were different molecular species from delayed rectifier K^+ channels contributing I_D, the population of these K^+ channels, which was the sum of open K^+ channels and blocked K^+ channels did not change. Using the model calculation of TBA blocking (Fig. 9D), it was concluded that this population decreased with TBA concentration. Most K^+ channels for I_D was converted to K^+ channels for I_{IN} in the hypertonic solutions and could be blocked by TBA efficiently before they were activated in the delayed kinetics. Although using squid giant axons it was difficult to prove directly that K^+ channels for I_{IN} were derived from same species of K^+ channel molecules, this conversion might be a useful proof that in hypertonic solutions same species of K^+ channels activated directly by the osmotic pressure and those activated after the successive closed states were equilibrated.

There may be several K^+ channels contributing the resting membrane potential (Goldstein et al. 2008) even in squid giant axons but there was no report about these channels for resting potential and only Kv families have been identified in squid neurons (Rosenthal et al. 1996; Clay and Kuzirian 2000). I used the traditional naming as squid delayed rectifier K^+ channels in place of specific molecular species as Kvs because there are several species possibly contributing squid delayed rectifier K^+ channels, which show sigmoidal

delayed activation kinetics, but all characteristics, including inactivation process, was not yet explained by K^+ channels identified in the cell body. Because K^+ channels contributing the resting membrane potential was not identified, squid delayed rectifier K^+ channels may work as these channels because the resting membrane potential was stable enough in hypertonic solutions to generate a usual conduction of action potential (Kukita 1982).

Considering the mechanism of the appearance of I_{IN}, similar traces showing the stepwise activation are recalled. This is a well-known reactivation kinetics after a short hyperpolarization following the activation Scheme 1 and was reported in squid giant axons (White and Bezanilla 1985) and in Shaker K^+ channels (Zagotta et al. 1994; Schoppa and Sigwoth 1998; Zhang and Sigworth 1998; Wang et al. 2004). This reactivation kinetics was explained by the sequential closed states (Scheme 1) in which K^+ channels were residing in the later closing state close to the open state were ready to open to present the instantaneous activation. Contrary to these experiments with a short hyperpolarization before the reactivation, in my experiment the membrane potential was hold at -80 mV throughout the experiments and the currents were measured after a sufficiently long preconditioning hyperpolarization of -100 or -150 mV and all K^+ channels were in early closing states. They were activated directly in hypertonic solutions at the membrane potential close to the resting potential by the aid of the osmotic shrinkage in hydrophilic parts coupling the voltage-sensor to the pore gate independently of states for the voltage sensors.

Osmosensitive K^+ channels have been recently reported (Schoenmakers et al. 1995) but they are activated by extracellular application of osmotic pressure less than 0.3 osm/l and sometimes they have been discussed in relation with stretch-activated channels (Hamill 2006; Hammami et al. 2009) in the condition of patch clamping. On the contrary, the experiment of intracellularly perfused squid giant axons were performed with osmolarities on both side of the membrane matched and the effect on membrane tension ignored and then osmotic pressure effects were observed even at the osmolarity above 4 osmol/l. My experiment was intended for the osmotic pressure to exert on the protein itself without accompanying the cell membrane expansion and shrinkage. In this case even if osmolarity-sensitive K^+ channels partly contributed to I_{IN}, the effect was saturated at a lower osmolarity. Furthermore the extracellular hypertonicity in squid giant axons only decreased periaxonal K^+ accumulation (Kukita and Yamagishi 1993; Kukita 1988) but not affect I_{IN}.

Previous investigators (Wagoner and Oxford 1987) did not find the initial jump component I_{IN} in concentrated electrolyte solutions because they obtained data in symmetrical K^+ concentrations, in which K^+ currents for the initial jump were linear if existed and were completely subtracted as the leakage component. Even in the asymmetrical K^+ concentrations, I found that I_{IN} was much smaller, which could be explained by the smaller size of electrolyte than nonelectrolytes. Indeed, as shown in Figs. 6 and 7, small nonelectrolytes such as ethylene glycol and urea caused much smaller I_{IN} but an interaction of charged particles electrolytes with hydrophilic region of K^+ channel might be quantitatively different from those of nonelectrolytes. K^+ current traces looks different from those by previous investigators (Zimmerberg et al. 1990) but I suppose that they might missing the data with the large leakage currents. They described in several places about large leakage currents and the difficulty of restoring the osmotic effect (Wagoner and Oxford 1987; Zimmerberg et al. 1990). On the other hand, I demonstrated that I_{IN} decreased in isotonic solutions after the hypertonic solutions were gradually returned to isotonic solutions. I think that the initial jump is a kind of leakage derived from delayed-rectifier K^+ channels directly opened by the osmotic pressure.

Acknowledgments I wish to thank Y. Nitani for collecting squid. I also thank members of the National Institute for Physiological Sciences for supporting this work. This work was supported by a grant from JSPS (12670053).

References

Armstrong CM, Hille B (1998) Voltage-gated ion channels and electrical excitability. Neuron 20:371–380

Clay JR (1991) A paradox concerning ion permeation of the delayed rectifier potassium ion channel in squid giant axons. J Physiol 444:499–511

Clay JR (2000) Determining K^+ channel activation curves from K^+ channel currents. Eur Biophys J 29:555–557

Clay JR, Kuzirian AM (2000) Localization of voltage-gated K^+ channels in squid giant axons. J Neurobiol 45:172–184

Conti F, Inoue I, Kukita F, Stühmer W (1984) Pressure dependence of sodium gating currents in the squid giant axon. Eur Biophys J 11:137–147

Cuello LG, Jogini V, Cortes DM, Perozo E (2010) Structural mechanism of C-type inactivation in K^+ channels. Nature 466:203–208

Doyle DA, Cabral JM, Pfuetzner RA, Kuo A, Gulbis JM, Cohen SL, Chait BT, MacKinnon R (1998) The structure of the potassium channel: molecular basis of K^+ conductance and selectivity. Science 280:69–77

French RJ, Shoukimas JJ (1981) Blockage of squid axon potassium conductance by internal tetra-*N*-alkylammonium ions of various size. Biophys J 34:271–291

Gilly WF, Armstrong CM (1982) Divalent cations and the activation kinetics of potassium channels in squid giant axons. J Gen Physiol 79:965–996

Goldstein SAN, Bockenhauer D, O'Kelly I, Zilberberg N (2008) Potassium leak channels and the KCNK family of two-P-domain subunits. Nat Rev Neurosci 2:175–184

Hamill OP (2006) Twenty odd years of stretch-sensitive channels. Pflügers Arch 453:333–351

Hammami S, Willumsen NJ, Olsen HL, Morera FJ, Lattore R, Klaerke DA (2009) Cell volume and membrane stretch independently control K^+ channel activity. J Physiol 587:2225–2231

Hille B (2001) Ion channels of excitable membranes, 3rd edn. Sinauer Associates, Sunderland

Hodgkin AL, Huxley AF (1952) Current carried by sodium and potassium ions through the membrane of the giant axon of *Loligo*. J Physiol 116:449–472

Jiang Y, Lee A, Chen J, Ruta V, Cadene M, Chait BT, MacKinnon R (2003a) X-ray structure of a voltage-dependent K^+ channel. Nature 423:33–41

Jiang Y, Ruta V, Chen J, Lee A, MacKinnon R (2003b) The principle of gating charge movement in a voltage-dependent K channel. Nature 423:42–48

Kukita F (1982) Properties of sodium and potassium channels of the squid giant axon far below 0°C. J Membr Biol 68:151–160

Kukita F (1988) Removal of periaxonal potassium accumulation in a squid giant axon by outward osmotic water flow. J Physiol 399:647–656

Kukita F (1997) Solvent-dependent rate-limiting steps in the conformational change of sodium channel gating in squid giant axons. J Physiol 498:109–133

Kukita F (2000) Solvent effects on squid sodium channels are attributable to movements of a flexible protein structure in gating currents and to hydration in a pore. J Physiol 522:357–373

Kukita F (2001) K^+ channel opened by a water activity decrease. Jpn J Physiol 51:183

Kukita F, Mitaku S (1993) Kinetic analysis of the denaturation process by alcohols of sodium channels in squid giant axon. J Physiol 463:523–543

Kukita F, Yamagishi S (1976) Prolongation of the action potential of squid giant axons in viscous solutions. Proc Jpn Acad 52:323–326

Kukita F, Yamagishi S (1979) Slowing of the time course of the excitation of squid giant axons in viscous solutions. J Membr Biol 47:303–325

Kukita F, Yamagishi S (1983) Effects of outward water flow on potassium currents in a squid giant axon. J Membr Biol 75:33–44

Li W, Aldrich RW (2004) Unique inner pore properties of BK channels revealed by quaternary ammonium block. J Gen Physiol 124:43–57

Rand RP (2004) Probing the role of water in protein conformation and function. Phil Trans R Soc Lond B 359:1277–1285

Rosenthal JJC, Vickery RG, Gilly WF (1996) Molecular identification of SqKv1A. A candidate for the delayed rectifier K channel in squid giant axon. J Gen Physiol 108:207–219

Schoenmakers ThJM, Vaudry H, Cazin L (1995) Osmo- and mechanosensitivity of the transient outward K^+ current in mammalian neuronal cell line. J Physiol 489:419–430

Schoppa NE, Sigwoth FJ (1998) Activation of Shaker potassium channels. I. Characterization of voltage-dependent transitions. J Gen Physiol 111:271–294

Shimizu H, Oiki S (2004) Asymmetric effect of nonelectrolytes on the gating of KcsA channel. Jpn J Physiol 54:s68

Sokolov S, Scheuer T, Cateral WA (2007) Gating pore current in an inherited ion channelopathy. Nature 446:76–78

Starace DM, Bezanilla F (2004) A proton pore in a potassium channel voltage sensor reveals a focused electric field. Nature 427:548–553

Starkus JG, Schlief T, Rayner MD, Heinemann SH (1995) Unilateral exposure of Shaker B potassium channels to hyperosmolar solutions. Biophys J 69:860–872

Tanaka T (1981) Gels. Sci Am 244:124–138

Tombola F, Pathak MM, Isacoff EY (2005) Voltage-sensing arginines in potassium channel permeate and occlude cation-selective pores. Neuron 45:379–388

Tombola F, Pathak MM, Gorostiza P, Isacoff EY (2007) The twisted ion-permeation pathway of a resting voltage-sensing domain. Nature 445:546–549

Van t'Hoff JH (1901) Osmotic pressure and chemical equilibrium. Nobel Prize Lecture in Chemistry. http://nobelprize.org/nobel_prizes/chemistry/laureates/1901/hoff-lecture.pdf

Wagoner PK, Oxford GS (1987) Cation permeation through the voltage-dependent potassium channel in the squid axon. Characteristics and mechanisms. J Gen Physiol 90:261–290

Wang S, Bondarenko VE, Qu Y, Morales MJ, Rasmusson RL, Strauss HC (2004) Activation properties of Kv4.3 channels: time, voltage and $[K]_O$ dependence. J Physiol 557:705–717

White MM, Bezanilla F (1985) Ionic and gating current studies. J Gen Physiol 85:539–554

Yahannan S, Hu Y, Zhou Y (2007) Crystallographic study of the tetrabutylammonium block to the KcsA K^+ channel. J Mol Biol 366:806–814

Zagotta C, Hosni T, Deadman J, Aldrich RW (1994) Shaker potassium channel gating II: transitions in the activation pathway. J Gen Physiol 103:279–319

Zhang J, Sigworth FJ (1998) Intermediate conductances during deactivation of heteromultimeric Shaker potassium channels. J Gen Physiol 112:457–474

Zimmerberg J, Parsegian VA (1986) Polymer inaccessible volume changes during opening and closing of a voltage-dependent ionic channel. Nature 323:36–39

Zimmerberg J, Bezanilla F, Parsegian VA (1990) Solute inaccessible aqueous volume change during opening of the potassium channel of the squid giant axon. Biophys J 57:1049–1064